



 Cite this: *RSC Adv.*, 2023, **13**, 22630

# Nanoengineering TiO<sub>2</sub> for evaluating performance in dye sensitized solar cells with natural dyes†

 Mohd Jahir Khan,<sup>a</sup> Ankesh Ahirwar,<sup>a</sup> Vandana Sirotiya,<sup>a</sup> Anshuman Rai,<sup>bc</sup> Sunita Varjani<sup>de</sup> and Vandana Vinayak \*<sup>a</sup>

The current study employs nanoengineering diatom and TiO<sub>2</sub> NPs to form diatom-Si-TiO<sub>2</sub> nanoengineered structures to fabricate a dye sensitized solar cell (DSSC) (*DsTnas*-DSSC). This was characterized and spin coated on a Fluorine-doped Tin Oxide (FTO) anode plate. The counter cathode was prepared by spin coating graphene oxide on a FTO glass plate and using Lugol's iodine as an electrolyte. The power density of *DsTnas*-DSSC was estimated with different natural dyes in comparison to conventional photosensitive ruthenium dye. It was found that the natural dyes extracted from plants and microalgae show significant power efficiencies in DSSC. The percentage efficiency of maximum power densities (PD<sub>max</sub>) of *DsTnas*-DSSC obtained with photosensitive dyes were 9.4% with synthetic ruthenium dye (control) and 7.19% > 4.08% > 0.72% > 0.58% > 0.061% from natural dyes found in *Haematococcus pluvialis* (astaxanthin) > *Syzygium cumini* (anthocyanin) > *Rosa indica* (anthocyanin) > *Hibiscus rosa-sinensis* (anthocyanin) > *Beta vulgaris* (betalains), respectively. Among all the natural dyes used, the PD<sub>max</sub> for the control ruthenium dye was 6.164 mW m<sup>-2</sup> followed by the highest in astaxanthin natural dye from *Haematococcus pluvialis* (5.872 mW m<sup>-2</sup>). Overall, the use of natural dye *DsTnas*-DSSC makes the fuel cell low cost and an alternative to conventional expensive, metal and synthetic dyes.

 Received 3rd May 2023  
 Accepted 17th July 2023

DOI: 10.1039/d3ra02927a

[rsc.li/rsc-advances](https://rsc.li/rsc-advances)

## 1. Introduction

The global energy crisis is an immense problem that needs an economical and facile solution for energy generation as well as storage. A huge increase in fossil fuel consumption results in global warming and environmental instability. To reduce our dependence on fossil fuels, much attention has been paid to renewable energy sources.<sup>1</sup> Development of photovoltaic technology is an important way to transform the Sun's energy into electrical energy which is the alternative source of energy on Earth.<sup>2,3</sup> Photovoltaic cells (PVCs) play a significant role in energy harvesting as they efficiently harvest clean and renewable solar energy to produce electricity without exploiting harmful substrates and rigorous production approaches.<sup>4-7</sup> Based on performance and cost effectiveness, the first-

generation solar cells, specifically PVC silicon solar cells, currently dominate the market. Though they are effective since the energy conversion is high, on the other hand, they are very expensive. One such type is dye sensitized solar cell (DSSCs) which is a third generation photovoltaic device invented in 1991 by Grätzel *et al.*<sup>8</sup> It is a promising technology with increasing interest as it has several advantages over conventional silicon solar cells. Fabrication process of DSSC is simple, inexpensive and can produce power even under low lighting conditions.<sup>9,10</sup> Generally, a DSSC consists of photo-anode which is made up of fluorine doped tin-oxide (FTO) or indium doped tin-oxide, (ITO) and a porous monocrystalline semiconductor TiO<sub>2</sub>, a photosensitive dye (commonly ruthenium dye), an electrolyte and counter electrode which also have FTO/ITO covered glass coated usually with a thin film of platinum or carbon.<sup>11,12</sup> Although DSSC has evolved in the past two decades but cost has remained a major barrier in commercialization. Due to this, scientist have been constantly working to lower down the cost of DSSC by incorporating nanomaterials and dyes which are cheap and photosensitive.

In nature diatoms are cheapest available biomaterials which have been demonstrated for their use in fuel cells *viz.*; DSSC, perovskite solar cells, microbial fuel cells.<sup>13-18</sup> They are photosynthetic microalgae with 3-dimensional porous cell wall called frustules which is made of hydrogenated amorphous silica.<sup>19,20</sup> It has nanoporous architecture which shows a vast diversity in shape and size and displays strong light scattering and trapping

<sup>a</sup>Diatom Nanoengineering and Metabolism Laboratory (DNM), School of Applied Science, Dr. Harisingh Gour Central University, Sagar, MP 470003, India. E-mail: kapilvinayak@gmail.com

<sup>b</sup>School of Engineering, Department of Biotechnology, Maharishi Markandeshwar University Ambala, Haryana, 133203, India

<sup>c</sup>State Forensic Science Laboratory, Haryana, Madhuban, 132037, India

<sup>d</sup>School of Energy and Environment, City University of Hong Kong, Tat Chee Avenue, Kowloon, 999077, Hong Kong

<sup>e</sup>Sustainability Cluster, School of Engineering, University of Petroleum and Energy Studies, Dehradun-248 007, Uttarakhand, India

† Electronic supplementary information (ESI) available. See DOI: <https://doi.org/10.1039/d3ra02927a>



capacity.<sup>21–23</sup> So the efficiency of DSSC can be enhanced by the integration of diatoms frustules onto anodes.<sup>24</sup>

In the present study, *DsTnas*-DSSC were synthesized by hydrothermal and co-precipitation method using diatom frustule rich in Si and TiO<sub>2</sub> to prepare photoanode in a DSSC which was characterised *via* various state of art instruments. Transition metals like ruthenium have been reported as sensitizers with high stability and absorption spectra. They give good efficiency in a DSSC, but due to their high cost and upscaling, it is a cause for concern. On the offset, natural pigments are photosensitisers which are cheap and nontoxic but face un-stability and short shelf life.<sup>25</sup> Among various natural dye tested in the present study astaxanthin (3,3'-dihydroxy-*b,b'*-carotene-4,4'-dione) biosynthesized from *Haematococcus pluvialis* has unique antioxidant properties.<sup>26,27</sup> On the other hand, anthocyanin (2-phenyl-1-benzopyrylium) and betalainins (betaxanthins and betacyanins) pigment from various flowers, fruits and roots are tested as source of natural photosensitizer dye in DSSC.

These natural pigment have hydroxyl groups which allow them to assemble on the TiO<sub>2</sub> film in a DSSC. Although these pigments are light and heat stable; a comparison of their use in DSSC will help to know the power efficiencies produced for the cheaper and efficient way of producing DSSC's.<sup>28</sup>

## 2. Materials and methods

Titanium(IV) oxide (TiO<sub>2</sub>), titania paste, ruthenium *cis*-bis(isothiocyanato) bis(2,2'-bipyridyl-4,4'-dicarboxylato), ruthenium(II), iodine solution was purchased from Sigma-Aldrich (St. Louis, MO, USA). FTO glass slides (25 × 25 × 2.2 mm) with sheet resistance 15 Ω sq<sup>-1</sup> were obtained from Techinstro, Maharashtra, India.

### 2.1. Synthesis of diatom (Si) doped TiO<sub>2</sub> nanostructures

Diatom frustules of *Nitzschia palea* were harvested from pure culture which was grown in *f/2* media under standard laboratory conditions.<sup>29,30</sup> The live diatoms were acid washed and the obtained empty frustules were cleaned and dried.<sup>18</sup> The diatom rich in Si were then doped with TiO<sub>2</sub> nanoparticles (NPs) *via* hydrothermal and co-precipitation method<sup>31</sup> with some modifications. Clean diatom frustules were washed, sieved and thermally annealed. Thereafter, diatom (Si) and TiO<sub>2</sub> NPs at ratio of 20 : 80 g% respectively were assorted individually in water. The, pH of TiO<sub>2</sub> NPs solution was calibrated to pH 11 while adding diatom rich Si dropwise. During preparation of *DsTnas*, solution was continuously stirred and agitated for 30–40 min. Once the reaction was completed a uniform suspension solution was formed which was cleaned and dried at temperature of near 24 h to form *DsTnas*.

### 2.2. Characterization of diatom (Si)-TiO<sub>2</sub> nanoarray structures (*DsTnas*)

The nanocomposite mixture *DsTnas* was characterized by spectroscopy and microscopic studies. FT-IR spectra of commercial TiO<sub>2</sub> NPs and *DsTnas* was done to determine the type of functional groups present in the samples. FT-IR spectra

(Model: Bruker ATR Alfa II FT-IR spectrometer (USA)) of the *DsTnas* was recorded as per protocol mentioned elsewhere<sup>32</sup> at the range of 400 cm<sup>-1</sup> to 4000 cm<sup>-1</sup>.

### 2.3. Extraction of natural dyes

Natural dyes rich in pigments anthocyanin, astaxanthin and betalainins were extracted from different plant materials namely Beet root (*Beta vulgaris*), Rose (*Rosa indica*), Hibiscus (*Hibiscus rosa-sinensis*), Indian blackberry (*Syzygium cumini*) and microalgae *Haematococcus pluvialis* (red stage). Each plant material (1 g) was washed properly with distilled water, dried and chopped into small pieces and kept in 10 mL of acetone. After extraction in acetone, solution was centrifuged at 3000 × *g* for 5 min, filtered and stored in dark at 4 °C. The pH of the different natural dyes was analysed. All dye solutions were further analysed for their respective UV-vis absorption spectra using UV-vis spectrophotometer (Lab India 3000 double beam).

Furthermore, thin layer chromatography was done for all the natural dyes. The pigment was extracted from all plant-based cells using 100% acetone and incubated at room temperature for overnight using hexane : acetone (7 : 3). The sample extracts were analysed by thin-layer chromatography (TLC) on silica gel plates (Himedia). Samples were spotted and air dried whereas the methanol : acetic acid : water (4 : 1 : 3) was taken as the mobile phase.

The natural dye which showed best performance in *DsTnas* was processed for LCMS as per protocol described in our earlier study.<sup>33</sup>

### 2.4. Fabrication of DSSCs anode and cathode

The six number of FTO glass slides with conductive side were selected as cathode/anode in a DSSCs. The FTO plates were rinsed with a mixture of ethanol and isopropanol for about 40 min in an ultrasonic bath. The rutile anatase was spin coated on anode of FTO plates so as to make a uniform homogenous layer (1000 rpm; 15 seconds). Further, a thin film of *DsTnas* was spin coated on the anatase layer. The thickness of the *DsTnas* film was measured using Ambios XP-2 Profilometer. The spin coated FTO plates were thereafter annealed for 2 hours at 400 °C so as to remove the organic particles and enhance film compactness and crystallinity. After cooling at room temperature, FTO control plate was immersed into standard ruthenium dye (3 × 10<sup>-4</sup> M) whereas the FTO test plates were dipped into five different natural pigment dyes and left for 2 h so that dyes gets properly adsorbed into films.<sup>8</sup> Finally, it was dried in air and ready to assemble with counter cathode for *DsTnas*-DSSC device preparation. The counter cathode was fabricated by spin coating of graphene oxide (GO) over conductive side of FTO glass plate and annealed (400 °C for 2 hour).

### 2.5. Assembling of diatom (Si)-TiO<sub>2</sub> dye sensitized solar cell (*DsTnas*-DSSC)

*DsTnas* coated anode was put over GO coated cathode in closed sandwich cell assembly so that conductive side of both the electrodes faced each other forming *DsTnas*-DSSC. The electrolyte, Lugol's iodine (50 mM) was introduced in between both



the electrodes and kept in a vacuum chamber to bubble out any air if present in between the electrodes. The edges of plates were then sealed. The closed sandwich assembly was thus circuited with wires and their connections were connected thereafter with the digital multimeter and characterised by SEM and its current voltage ( $I$ - $V$ ) curve plotted (ESI Fig. 1†).

**2.5.1. Measurement of voltage, current and power density of a *DsTnas*-DSSC.** The prepared *DsTnas*-DSSC assembly was irradiated with the white LED at the intensity of 20.2 Klux. Thereafter the open circuit voltage, operating voltage, current and maximum power density (PD<sub>max</sub>) of the fabricated DSSCs with ruthenium dye and different natural extracted pigment dyes were determined by digital multimeter (Model: MECO, 171B, India) individually using external resistance (1  $\Omega$  to 100 k $\Omega$ ).<sup>34</sup>

### 3. Results and discussion

#### 3.1. Characterization of diatom (Si)-TiO<sub>2</sub> nanostructures by SEM and EDX

To fabricate anode of DSSC, TiO<sub>2</sub> NPs (Fig. 1A) are doped on diatom frustules (Fig. 1B). The TiO<sub>2</sub> NPs are doped inside the nanopores of diatom to form *DsTnas* nanocomposites (Fig. 1C). The anatase (Fig. 1D) is spin coated on FTO followed up by layering of *DsTnas* nanocomposite on it (Fig. 1E). It was found that SEM image of anatase appeared as cubes like single crystal structures and TiO<sub>2</sub> NPs as nanoclusters. When the TiO<sub>2</sub> NPs were functionalised within diatoms they formed diatom (Si)-TiO<sub>2</sub> nanoarray structures with TiO<sub>2</sub> NPs well-arranged inside nanopores of diatom frustules well in coherence to earlier reported studies.<sup>20</sup>

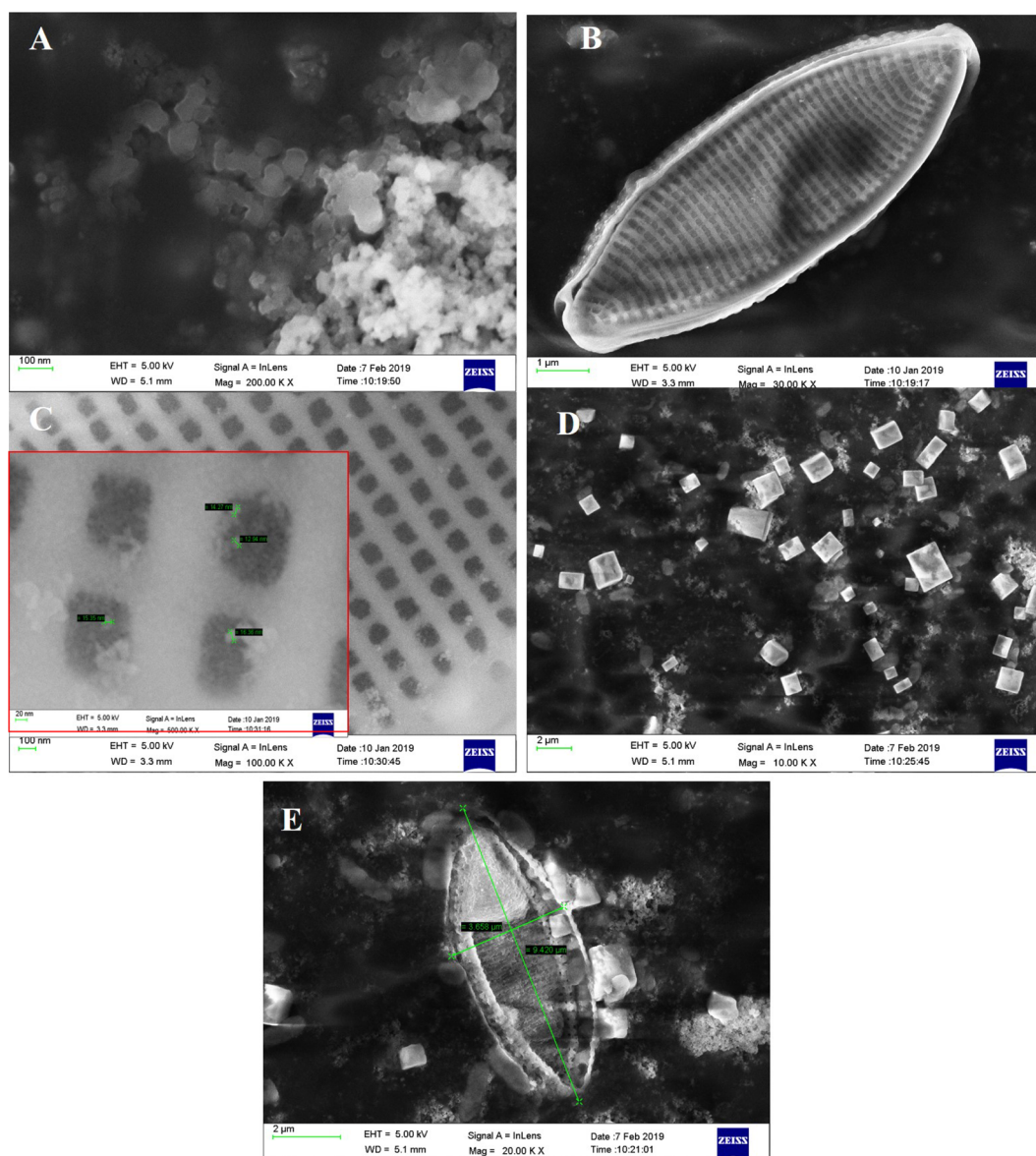


Fig. 1 Morphological transformation shown via SEM images (A) TiO<sub>2</sub> NPs; (B) diatom; (C) diatom frustules showing pores embedded with TiO<sub>2</sub> NPs; (D) titania single crystal and (E) nanocomposite of diatom Si-TiO<sub>2</sub> NPs.



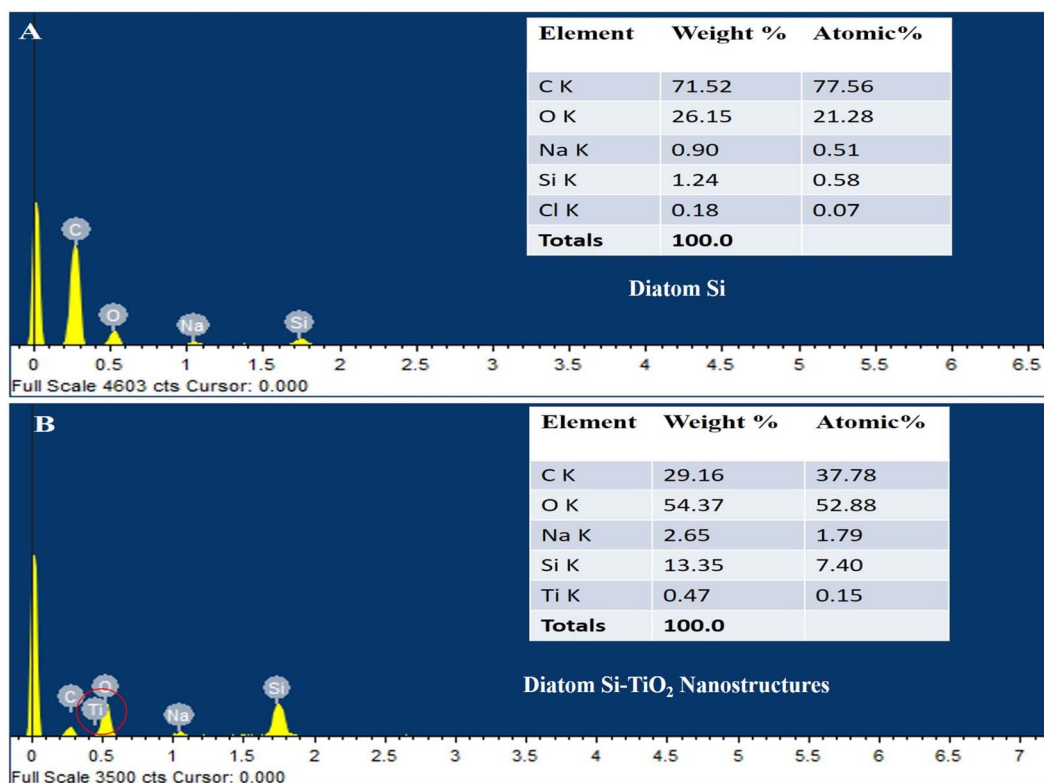


Fig. 2 Scanning electron microscopy–energy dispersive X-ray analysis (SEM–EDX) of elemental composition of (A) diatom Si and (B) diatom Si–TiO<sub>2</sub> NPs.

The elemental composition of diatom and diatom (Si)–TiO<sub>2</sub> nanoarray structures *DsTnas* were determined by energy-dispersive X-ray spectrometer (EDX) (Fig. 2A and B). The results showed that the diatoms had chemical compositions rich in C, O, Na, Si and Cl while diatom (Si)–TiO<sub>2</sub> nanoarray structures displayed additional Ti, thus revealing that the diatoms were successfully doped with TiO<sub>2</sub> NPs. Further, EDX of the assembled *DsTnas*-DSSC using standard ruthenium before its operation and without electrolyte (KI) and during operation in the presence of electrolyte potassium iodide (KI) showed altered chemical composition as well as incorporation of iodine ions due to the KI as electrolyte (ESI Fig. 2A and B†).

### 3.2. TEM analysis

It has been reported that diatoms frustules are rich in silica.<sup>18,35</sup> Doping of diatoms (Si) with TiO<sub>2</sub> NPs resulted in diatom (Si)–TiO<sub>2</sub> nanoarray structures (*DsTnas*) which was also studied *via* TEM for high resolution study of nanoparticles nanoarray structures (Fig. 3 and ESI Fig. 3†). The TEM study showed an accurate deposition of TiO<sub>2</sub> in diatom forming *DsTnas*. Further, the formation of these complex nanostructures was very well concordance with the XRD results. The TEM images of the TiO<sub>2</sub> NPs showed that these NPs were not only spherical but also irregular in size and its distribution (Fig. 3A). Some NPs are large and spherical while others are small in size with different shapes.<sup>36</sup> Further Fig. 3B shows selected area electron diffraction (SAED) pattern which is in accordance to the crystal plane structure of the nanostructures (Si–TiO<sub>2</sub> NPs) (Fig. 3B). The HR-

TEM further showed the well-arranged lattice fringes of the nanostructures (Si–TiO<sub>2</sub> NPs) (Fig. 3C). The '*d*' spacing of the lattice fringe was in the range of 0.45 nm (Fig. 3C). However, the average size of TiO<sub>2</sub> NPs was ~19.01 nm (Fig. 3D).<sup>37</sup>

### 3.3. Characterisation of functional groups and crystallographic study

**3.3.1. FT-IR characterization.** The FT-IR spectra of TiO<sub>2</sub> and *DsTnas* was done at wavenumbers range of 500–4000 cm<sup>-1</sup> (Fig. 4A and B). IR spectrum classify the chemical bonds as well as functional group present in the samples. The broadest band was seen at 3500 cm<sup>-1</sup> which is due to O–H stretching of Ti–OH bonds. Strong absorption peak at 500–1100 cm<sup>-1</sup> were seen which represented the Ti–O and Ti–O–Ti bonds. This was probably due to the vibrations arising due to bending and stretching between Ti–OH and Ti–O–Ti (Fig. 4A). There are sharp characteristic absorption bands around 600 cm<sup>-1</sup> which corresponds to the rutile phase of TiO<sub>2</sub> (Fig. 4A).<sup>38,39</sup> The FT-IR spectrum of *DsTnas* showed that position 810 cm<sup>-1</sup> corresponded to the Si bands which was due to the Si–O–Si vibrations.<sup>40</sup> It was observed that siloxane vibrations at 1112 cm<sup>-1</sup> were formed due to (SiO)<sub>n</sub> groups<sup>41,42</sup> revealing that the silica content in diatom formed *DsTnas* (Fig. 4B).

**3.3.2. XRD characterization.** The TiO<sub>2</sub> NPs and *DsTnas* were further evaluated by XRD technique (Fig. 4C and D). The XRD pattern of commercial TiO<sub>2</sub> NPs is depicted in Fig. 4C. The broad diffraction line of the sample is related to the nanocrystalline anatase phase. The results of formation of strong peaks at about



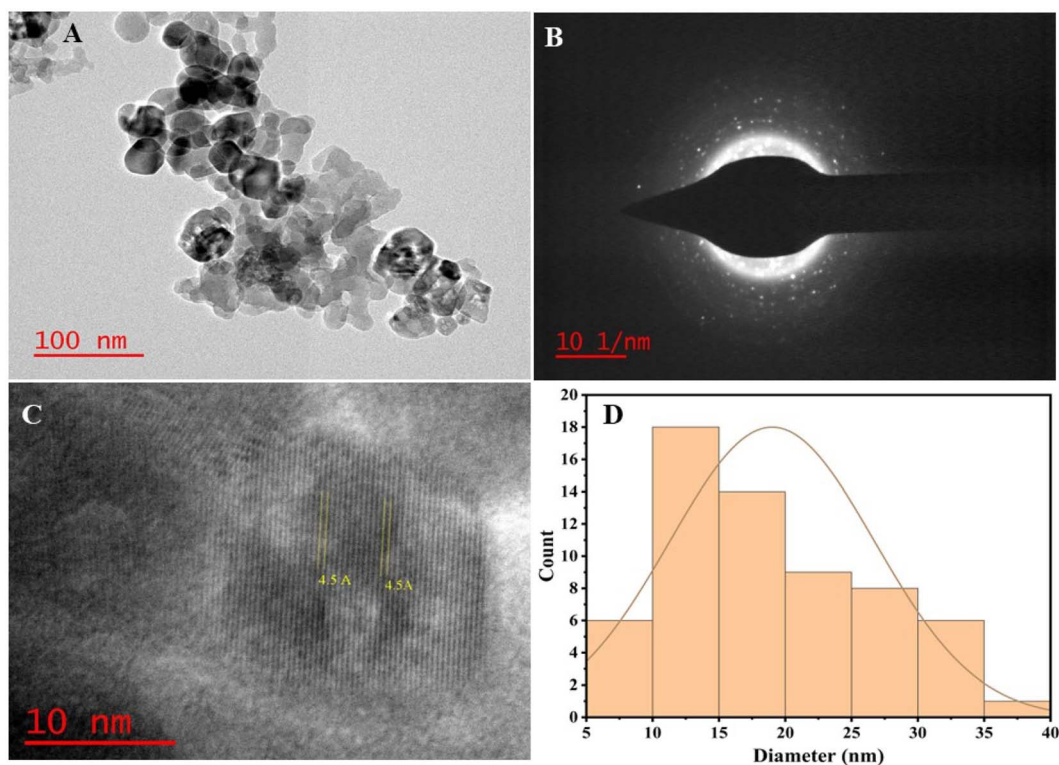


Fig. 3 (A) TEM image of diatom-Si-TiO<sub>2</sub> NP; (B) HR-TEM image of diatom-Si-TiO<sub>2</sub> NP (C) selected area electron diffraction (SAED) pattern of diatom-Si-TiO<sub>2</sub> NP for HR-TEM showing *d* spacing of 0.45 nm and (D) average size of TiO<sub>2</sub> NPs.

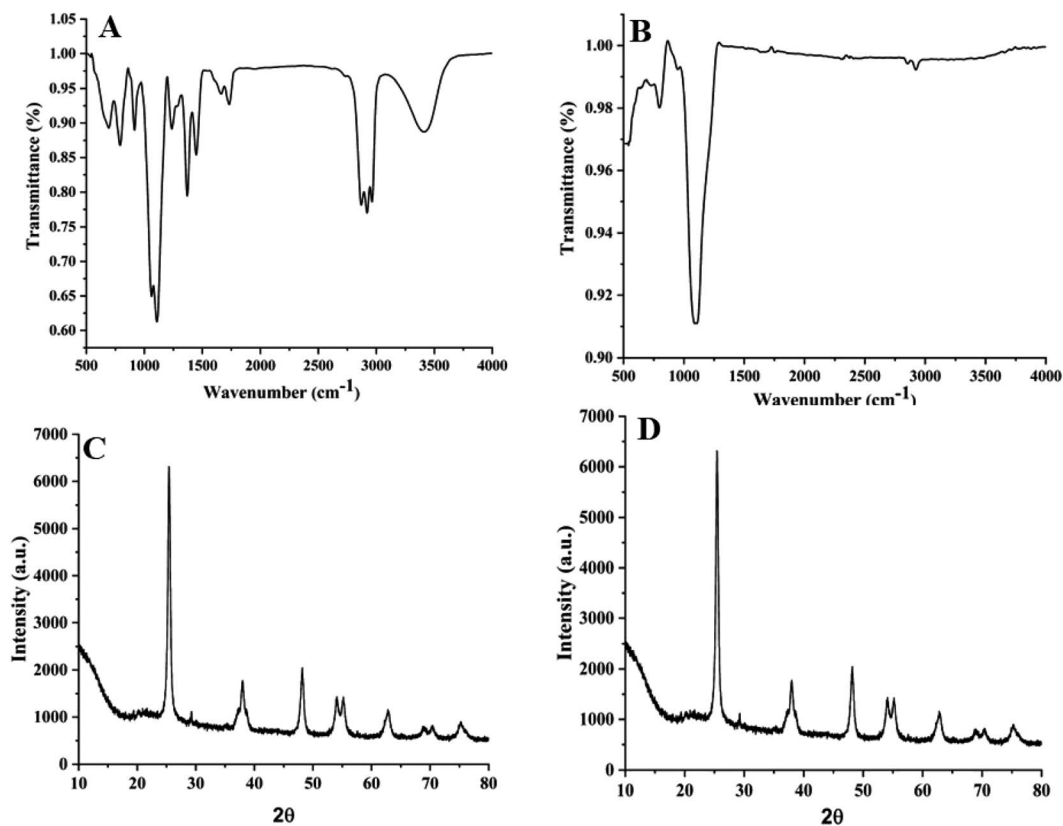


Fig. 4 FTIR spectra of (A) TiO<sub>2</sub> NPs and (B) diatom-Si doped TiO<sub>2</sub> NPs and X-ray diffraction patterns of (C) TiO<sub>2</sub> NPs and (D) diatom-Si doped TiO<sub>2</sub> NPs.



$2\theta = 25.2^\circ, 37.8^\circ, 47.7^\circ, 54.7^\circ, 63.0^\circ$  and  $68.9^\circ$  were well in accordance with indices at (101), (004), (200), (211), (204) and (116) which were part of anatase phase of titania (Fig. 4C).<sup>43</sup> The XRD patterns in both TiO<sub>2</sub> NPs and Si doped TiO<sub>2</sub> NPs showed sharp and strong peak at  $2\theta = 25^\circ$  of anatase phase. XRD phase identification patterns showed some minor peaks due to rutile phase. The XRD patterns of Si-TiO<sub>2</sub> NPs are essentially crystalline structure which can be accomplished from the broad characteristic diffraction peak between  $2\theta$  value of 20–80° (Fig. 4D).<sup>44</sup> The results are well in concordance with earlier reported from the literature which show that the absence of Si, does not change the crystalline structure of TiO<sub>2</sub>, therefore the XRD spectra of TiO<sub>2</sub> and diatom-Si doped TiO<sub>2</sub> NPs was almost similar. The optical, material and mechanical properties of diatom thus makes them as naturally available nanomaterial besides being rich in value added compounds mainly crude oil and fucoxanthin.<sup>45,46</sup>

### 3.4. UV-vis spectroscopy

Once the *DsTnas* was synthesized and characterised to serve as anode of the DSSC, it was necessary to test different natural dyes which would be acting as photosensitive dyes in the DSSC. The natural dyes extracted from Beet root (*Beta vulgaris*), Rose (*Rosa indica*), hibiscus (*Hibiscus rosa-sinensis*), Indian blackberry (*Syzygium cumini*) and microalgae *H. pluvialis* (red stage) were analysed for their pH which was 4, 3.5, 6.4, 4.1, 4.2 respectively and 2.9 for synthetic ruthenium dye (standard) (ESI Fig. 4†). Further, the absorbance peaks of each natural dye and standard ruthenium dye were analysed *via* UV-vis spectrophotometer.

The absorption maxima of *Rosa indica*, *Syzygium cumini*, *Hibiscus rosa-sinensis*, *H. pluvialis*, *Beta vulgaris* and ruthenium was 534 nm, 522 nm, 480 nm, 490 nm, 474 nm and 505 nm, respectively (Fig. 5A) which is in coherence with the existing studies.<sup>47–51</sup> The appearance of absorption spectra in the range between 454 and 540 nm indicated high concentration of anthocyanin isomers present in these extracted natural dyes.<sup>52,53</sup> It was found that the *Hibiscus rosa-sinensis* displayed two wide absorption peaks at 430 nm and 540 nm.<sup>54</sup> Similarly astaxanthin from *H. pluvialis* shows one peak at 490 nm which is in concordance with the reported studies.<sup>55,56</sup> The shifts in the absorption peaks of the different pigment dyes were probably due to varied chemical structure of these natural pigment dyes. Further, the TLC studies have shown diverse separation of anthocyanins, astaxanthin and betalains in different TLC plates (Fig. 5B). TLC fraction of *Hibiscus rosa-sinensis* showed a single spot with  $R_f$  value 0.40 identified as anthocyanin as per earlier reported work where  $R_f$  value of 0.32 was obtained using solvent mixture HCl : acetic acid : water.<sup>57</sup> Similarly, TLC of *Syzygium cumini* fruit showed a single spot with  $R_f$  value of 0.31 as anthocyanin in consistency with reported literature wherein  $R_f$  value of 0.30 was obtained using methanol : formic acid : water was used as mobile phase.<sup>58</sup> On the offset, TLC of *H. pluvialis* separated pigments such as primary xanthophylls astaxanthin monoester, astaxanthin diester, adonirubin ester, echinenone, adonixanthin diester,  $\beta$ -carotene with  $R_f$  value of 0.46, 0.51, 0.70, 0.72, 0.80, 0.84, 0.85 respectively. In a similar study conducted on microalga *Bracteacoccus aggregatus* BM5/15 using mobile phase hexane : chloroform : benzene, the separated

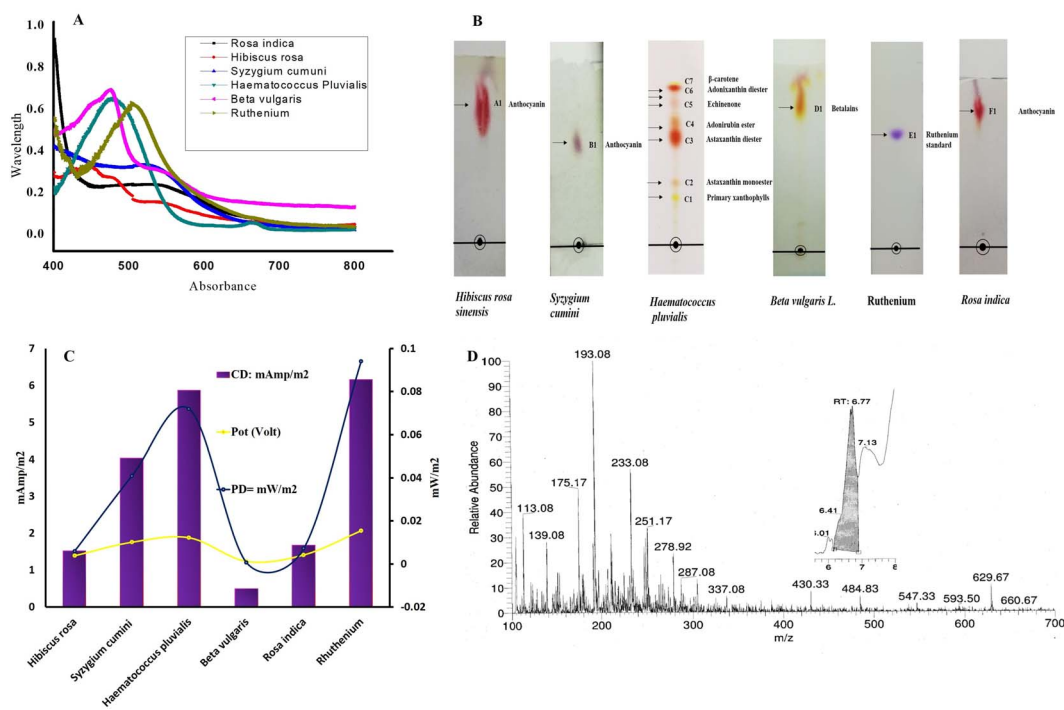


Fig. 5 Characterisation of natural dyes *Hibiscus rosa-sinensis*; *Syzygium cumini*; *Haematococcus pluvialis*; *Beta vulgaris*; ruthenium and *Rosa indica* by (A) UV-vis spectroscopy, (B) thin layer chromatography (C) collective maximum current and  $PD_{max}$  of diatom rich Si-TiO<sub>2</sub> nanoarray structures-dye sensitized solar cells using different plant dyes and their comparison with control (ruthenium) and (D) LCMS of dye (astaxanthin) from *H. pluvialis*.



pigments such as primary xanthophylls, astaxanthin mono-ester, astaxanthin diester, adonirubin ester, echinenone, adonixanthin diester,  $\beta$ -carotene displayed  $R_f$  value of 0.04, 0.24, 0.56, 0.44, 0.59, 0.80, 0.98, respectively.<sup>59</sup>

TLC fraction of *Beta vulgaris* L. showed a single spot with  $R_f$  value of 0.5, identified as betacyanin. In a similar study on *Beta vulgaris* using a mixture of isopropanol : ethanol : water : acetic acid as mobile phase, betacyanin displayed  $R_f$  value of 0.48.<sup>60</sup> The TLC fraction of ruthenium standard (Sigma Aldrich) showed single spot with  $R_f$  value of 0.50 in support with earlier reported studies.<sup>61</sup> Additionally, the TLC fraction of *Rosa indica* showed a single spot of anthocyanin with  $R_f$  value of 0.42 in concordance with similar pigment with  $R_f$  value of 0.46 when 0.1% formic acid in aqueous solution and 0.1% formic acid acetonitrile was used as mobile phase.<sup>62</sup>

### 3.5. Current and power density of *DsTnas*-DSSC

The current density of *DsTnas*-DSSC using different dyes was analysed to evaluate its performance using range of resistance. The best changes in potential of *DsTnas*-DSSC with respect resistance (10  $\Omega$  to 100 k $\Omega$ ) using dyes are shown Fig. 5C and that from resistance 10 k $\Omega$  to 120 k $\Omega$  in ESI Fig. 5† followed a similar pattern. The open circuit voltage was highest for *H. pluvialis* (0.92 mV) and lowest for *Beta vulgaris* (0.237 mV) compared to 0.732 mV of standard ruthenium (ESI Fig. 6†). The obtained potential was used to calculate current density using Ohm's law. The electrochemical data showed that the percentage efficiency of PD<sub>max</sub> of *DsTnas*-DSSCs was 9.4% with control ruthenium dye. Among the natural pigment dyes that were used as photosensitive dyes in a *DsTnas*-DSSC for generating electric current, it was seen that percentage efficiency of PD<sub>max</sub> from astaxanthin dye extracted from *H. pluvialis* was 7.19%. Further, natural dyes rich in anthocyanin from *Syzygium cumini* showed percentage efficiency of PD<sub>max</sub> 4.08%. The natural dyes from other plant parts viz.; *Beta vulgaris*, *Rosa indica* and *Hibiscus rosa-sinensis* showed percentage efficiency of PD<sub>max</sub> < 1%. The PD<sub>max</sub> of *DsTnas*-DSSCs with different natural dyes were 6.164, 5.872, 4.04 1.676, 1.524, 0.492 mW m<sup>-2</sup> at 50 k $\Omega$  for ruthenium dye (standard as control) and extracted dyes from *H. pluvialis*, *Syzygium cumini*, *Rosa indica* and *Hibiscus rosa-sinensis* and *Beta vulgaris*, respectively (Fig. 5C). These data showed that the ruthenium is most efficient dye followed by extracts of astaxanthin from *H. pluvialis* and anthocyanin from *Syzygium cumini* dye in *DsTnas*-DSSC. On the offset, anthocyanin natural dyes extracted from *Rosa indica* and *Hibiscus rosa-sinensis* and betalains from *Beta vulgaris* displayed least performance. In this study, an efficient and stable DSSC in which diatom *DsTnas* serves as an advantages material can be applied in the preparation of various cheap and facile DSSCs.

Since astaxanthin from *H. pluvialis* shows promising photosensitizer properties in the present fabricated *DsTnas*-DSSC, ITS LCMS was done. Fig. 5D represents the LCMS of astaxanthin from *H. pluvialis* as only pigment present in its mono and diester form and thus LCMS showed its diverse ester compounds. The chromatogram shows detection of  $m/z$  values at 287.92–284.3 denoting astaxanthin, which was comparative to studies

in *Chlorella vulgaris*.<sup>63</sup> Similarly other compounds at  $m/z$  like 233.08–233 for presence of halocynthiaxanthin, at  $m/z$  of 251.17–251 denoting (3*S*,4*R*,30*R*)-4-hydroxyalloxanthin as seen in *Isochrysis galbana*.<sup>64</sup> Furthermore,  $m/z$  of 593.50–539 was identified as 53-7,8,7',8'-tetradrhydroastaxanthin as in other studies on *H. pluvialis*.<sup>65</sup> The *DsTnas* enhanced the electron extraction due to photonic property of diatom nanopores which promoted the formation of compact uniform and homogenous layer. The DSSCs performance significantly improved within the nanoarray diatom-Si structure embedded with TiO<sub>2</sub>. The large active surface area of diatom Si-TiO<sub>2</sub> nanoarray structure helps in providing resonance in visible spectral range, thus increased possibility of photon induced electron excitation. Additionally, more electrolyte and dye bound to the material increased photon adsorptions from solar energy thus enhanced the DSSC efficiency.<sup>66</sup>

Thus, from these studies, it is evident that diatoms are being used in solar cells, batteries and electroluminescent technology.<sup>66</sup> The solar-current conversion efficiency of the DSSC, a low-cost photovoltaic device, is approximately 12%. Ruthenium-based dye particles serve an important function when they are attached to crystalline anatase TiO<sub>2</sub> films that serve as photoanodes and are immersed in electrolyte. The dye in the DSSC transfers electrons to the TiO<sub>2</sub> film when exposed to sunlight thus creating electron hole pairs. Electrons pass through the TiO<sub>2</sub> layer to conductive FTO glass to the appliance or load, and back to the electrolyte. To fill the dye's electron hole, the electrolyte releases electrons.<sup>67</sup> Diatom frustule was employed by Jeffryes *et al.* in DSSC.<sup>68</sup> They connected the composite frustules to the dye-TiO<sub>2</sub> layer after culturing TiO<sub>2</sub> into the frustules. The transparent frustule pores allows the penetration of photons thus allowing light scattering, light reflection and light focusing so as to direct photons to the dye.<sup>69,70</sup> A thinner photoanode layer produced by improved photonic capture lowers the electron diffusion distance, boosts efficiency, and lowers the cost of production. Because the titanium put into the frustule is of poor quality and the TiO<sub>2</sub> is primarily dispersed along the pores, the effectiveness of the TiO<sub>2</sub>-frustule layer can be increased. In a later work, Jeffryes *et al.*,<sup>66</sup> created composite frustules with a homogeneous TiO<sub>2</sub> coating layer using a deposition process. The effectiveness of the photoanode is increased by 3.7% with the addition of the composite frustule.<sup>66,68</sup> Thus, it is clear that innovative diatom processing techniques can enhance the functionality of diatom devices. Gautam *et al.*,<sup>34</sup> has further demonstrated that TiO<sub>2</sub> NPs were doped on diatom by two-way cell culturing methods and direct doping methods using sol-gel method with additional direct incubation with Ag nanoparticles (Ag NPs) so as to obtain diatom (Si)-TiO<sub>2</sub> nanotubes doped on DSSC.<sup>71</sup> The DSSC doped with diatoms TiO<sub>2</sub> nanotubes *via* direct doping with Ag NPs has shown facile power efficiency of 8.45% which was nearly close to that from two way culturing method (9.45%).<sup>34,71</sup>

However, in this work, we show how dye-sensitized solar cells using diatom-Si-TiO<sub>2</sub> have better light trapping. According to the electrochemical data, the percentage efficiency of maximum power density (PD<sub>max</sub>) of the *DsTnas*-DSSCs was with synthetic dye ruthenium dye (9.4%) and 7.19% from organic dye astaxanthin from *H. pluvialis* which is equally good in terms of its cost



effectiveness. A difficult but possible commercial objective for the current DSSC technology is to get efficiency exceeding 15%. By increasing the light responsiveness of the sensitizers in the near IR spectral region, future advancements will concentrate on the short circuit current ( $J_{SC}$ ). Thus an easy and flexible new method is necessary to attain high efficiency to create novel ligands that result in the creation of new dyes or ruthenium sensitizers.<sup>72</sup>

## 4. Conclusion

In this study diatom *DsTnas* were synthesized, characterized via SEM, TEM, XRD, FTIR, UV-vis and assembled into DSSC. The astaxanthin, anthocyanin and betalains natural dyes were treated as photosensitizer dyes and compared with standard ruthenium dye. It was seen that astaxanthin from *Haemato-coccus pluvialis* displayed highest power density (5.872 mW m<sup>-2</sup>) among other anthocyanins and betalains natural dyes from different plant sources after standard synthetic ruthenium dye (6.164 mW m<sup>-2</sup>) used conventionally in DSSCs. This definitely can lead towards economical fabrication of DSSC thus depleting the cost of expensive ruthenium dye. This is probably because of enhanced charge transfer from the natural dye molecule and the diatom *DsTnas* surfaces. Pigments are produced in large quantities in plants. These photosensitive natural dyes possess hydroxyl groups which allow the binding to the TiO<sub>2</sub> layer. Thus, from an economic aspect, natural dyes can be a good choice to fabricate DSSCs provided the shelf life of these dyes are increased as they are very sensitive to degradation. On the offset, among these natural dyes astaxanthin in esterified form shows more stability compared to anthocyanin or any other plant pigment thus can be a better alternate after ruthenium to be used in DSSC. This study is important as it opens the use of low-cost natural pigment dyes as photosensitizers to run DSSCs for electricity production.

## Data availability

Data would be available on request.

## Author contributions

MJK: literature review, writing-original draft, data curation; AA: data curation; VS: data curation; AR: data curation; SV: review; VV: conceptualization; supervision; writing – original draft; review & editing; Funding acquisition.

## Conflicts of interest

The authors declare that they have no known competing financial interests or personal relationships that could have appeared to influence the work reported in this paper.

## Acknowledgements

MJK thanks DST-Nanomission for Postdoc Fellowship. VV gratefully acknowledge to DST-Nanomission (Government of

India) project no. (SR/NM/NT-1090/2014(G)) and CEFIPRA Indo French project no. 7133/2020 for funding support.

## References

- 1 M. Mourya, M. J. Khan, A. Ahirwar, B. Schoefs, J. Marchand, A. Rai, S. Varjani, K. Rajendran, J. R. Banu and V. Vinayak, *Fuel*, 2022, **314**, 122738.
- 2 G. K. Singh, *Energy*, 2013, **53**, 1–13.
- 3 A. Hagfeldt, G. Boschloo, L. Sun, L. Kloo and H. Pettersson, *Chem. Rev.*, 2010, **110**, 6595–6663.
- 4 J. R. Benemann, *Energy Convers. Manage.*, 1997, **38**, S475–S479.
- 5 Y. Watanabe and D. O. Hall, *Energy Convers. Manage.*, 1996, **37**, 1321–1326.
- 6 S. Ashina, J. Fujino, T. Masui, T. Ehara and G. Hibino, *Energy Policy*, 2012, **41**, 584–598.
- 7 M. Wang, N. Chamberland, L. Breau, J. E. Moser, R. Humphry-Baker, B. Marsan, S. M. Zakeeruddin and M. Gratzel, *Nat. Chem.*, 2010, **2**, 385–389.
- 8 B. O'Regan and M. Grätzel, *Nature*, 1991, **353**, 737–740.
- 9 S. Mathew, A. Yella, P. Gao, R. Humphry-Baker, B. F. E. Curchod, N. Ashari-Astani, I. Tavernelli, U. Rothlisberger, M. K. Nazeeruddin and M. Grätzel, *Nat. Chem.*, 2014, **6**, 242.
- 10 D. Joly, L. Pellejà, S. Narbey, F. Oswald, J. Chiron, J. N. Clifford, E. Palomares and R. Demadrille, *Sci. Rep.*, 2014, **4**, 4033.
- 11 Y. Gao, J. Zhu, H. An, P. Yan, B. Huang, R. Chen, F. Fan and C. Li, *J. Phys. Chem. Lett.*, 2017, **8**, 1419–1423.
- 12 N. T. R. N. Kumara, A. Lim, C. M. Lim, M. I. Petra and P. Ekanayake, *Renewable Sustainable Energy Rev.*, 2017, **78**, 301–317.
- 13 M. J. Khan, S. Das, V. Vinayak, D. Pant and M. Ghangrekar, *Chemosphere*, 2022, **291**, 132841.
- 14 A. Rai, M. J. Khan, A. Ahirwar, R. Deka, N. Singh, B. Schoefs, J. Marchand, S. Varjani and V. Vinayak, *Int. J. Hydrogen Energy*, 2022, **47**, 42099–42121.
- 15 M. J. Khan, V. J. Suryavanshi, K. B. Joshi, P. Gangadharan and V. Vinayak, in *Handbook of Algal Biofuels*, Elsevier, 2022, pp. 363–384.
- 16 V. Vinayak, M. J. Khan, S. Varjani, G. D. Saratale, R. G. Saratale and S. K. Bhatia, *J. Biotechnol.*, 2021, **338**, 5–19.
- 17 M. J. Khan, N. Singh, S. Mishra, A. Ahirwar, F. Bast, S. Varjani, B. Schoefs, J. Marchand, K. Rajendran and J. R. Banu, *Chemosphere*, 2022, **288**, 132589.
- 18 M. J. Khan, A. Pugazhendhi, B. Schoefs, J. Marchand, A. Rai and V. Vinayak, *Chemosphere*, 2022, **291**, 132692.
- 19 M. J. Khan, R. Singh, K. B. Joshi and V. Vinayak, *RSC Adv.*, 2019, **9**, 22410–22416.
- 20 S. Gautam, M. Kashyap, S. Gupta, V. Kumar, B. Schoefs, R. Gordon, C. Jeffries, K. B. Joshi and V. Vinayak, *RSC Adv.*, 2016, **6**, 97276–97284.
- 21 T. Fuhrmann, S. Landwehr, M. El Rharbi-Kucki and M. Sumper, *Appl. Phys. B: Lasers Opt.*, 2004, **78**, 257–260.
- 22 J. Romann, J.-C. Valmalette, M. S. Chauton, G. Tranell, M.-A. Einarsrud and O. Vadstein, *Sci. Rep.*, 2015, **5**, 17403.





- 23 J. Toster, K. S. Iyer, W. Xiang, F. Rosei, L. Spiccia and C. L. Raston, *Nanoscale*, 2013, **5**, 873–876.
- 24 K. Shin, Y. Jun, J. H. Moon and J. H. Park, *ACS Appl. Mater. Interfaces*, 2010, **2**, 288–291.
- 25 G. Richhariya, A. Kumar, P. Tekasakul and B. Gupta, *Renewable Sustainable Energy Rev.*, 2017, **69**, 705–718.
- 26 V. Sirotiya, A. Ahirwar, M. Mourya, M. J. Khan, A. Rai, R. Kwatra, A. K. Sharma, B. Schoefs, J. Marchand and S. Varjani, *Phytochem. Rev.*, 2022, 1–26.
- 27 A. Ahirwar, K. Kesharwani, R. Deka, S. Muthukumar, M. J. Khan, A. Rai, V. Vinayak, S. Varjani, K. B. Joshi and S. Morjaria, *J. Biotechnol.*, 2022, **349**, 32–46.
- 28 N. Prabavathy, R. Balasundaraprabhu, A. S. Kristoffersen, G. Balaji, S. Prasanna, K. Sivakumaran, M. Kannan, S. R. Erga and D. Velauthapillai, *Optik*, 2021, **227**, 166053.
- 29 M. J. Khan, R. Singh, K. Shewani, P. Shukla, P. Bhaskar, K. B. Joshi and V. Vinayak, *Sci. Rep.*, 2020, **10**, 1–11.
- 30 V. Vinayak, R. Gordon, S. Gautam and A. Rai, *Adv. Sci. Lett.*, 2014, **20**, 1256–1267.
- 31 C. C. Kee, B. C. Ang and H. S. C. Metselaar, *Ceram. Int.*, 2021, **47**, 4803–4812.
- 32 A. Ahirwar, M. J. Khan, V. Sirotiya, M. Mourya, A. Rai, B. Schoefs, J. Marchand, S. Varjani and V. Vinayak, *BioEnergy Res.*, 2022, 1–14.
- 33 M. Mourya, M. J. Khan, V. Sirotiya, A. Ahirwar, B. Schoefs, J. Marchand, S. Varjani and V. Vinayak, *RSC Adv.*, 2023, **13**, 17611–17620.
- 34 S. Gautam, M. Kashyap, S. Gupta, V. Kumar, B. Schoefs, R. Gordon, C. Jeffryes, K. B. Joshi and V. Vinayak, *RSC Adv.*, 2016, **6**, 97276–97284.
- 35 M. J. Khan, R. Gordon, S. Varjani and V. Vinayak, *Sci. Total Environ.*, 2022, **823**, 153667.
- 36 R. Tamayo, R. Espinoza-González, F. Gracia, U. P. Rodrigues-Filho, M. Flores and E. Sacari, *Nanomaterials*, 2019, **9**, 1–16.
- 37 D. Zhang and Z. J. Liu, *Appl. Mech. Mater.*, 2010, **26–28**, 835–838.
- 38 V. G. Erkov, S. F. Devyatova, E. L. Molodstova, T. V. Malsteva and U. A. Yanovskii, *Appl. Surf. Sci.*, 2000, **166**, 51–56.
- 39 N. D. Abazović, M. I. Čomor, M. D. Dramićanin, D. J. Jovanović, S. P. Ahrenkiel and J. M. Nedeljković, *J. Phys. Chem. B*, 2006, **110**, 25366–25370.
- 40 Y.-K. Lu and X.-P. Yan, *Anal. Chem.*, 2004, **76**, 453–457.
- 41 L. Bois, A. Bonhommé, A. Ribes, B. Pais, G. Raffin and F. Tessier, *Colloids Surf., A*, 2003, **221**, 221–230.
- 42 V. Kumar, M. Kashyap, S. Gautam, P. Shukla, K. B. Joshi and V. Vinayak, *J. Biosci.*, 2018, **43**, 717–729.
- 43 J. Lei, X. Li, W. Li, F. Sun, D. Lu and Y. Lin, *J. Solid State Electrochem.*, 2012, **16**, 625–632.
- 44 S. Azadi, A. Karimi-Jashni, S. Javadpour and L. Mahmoudian-Boroujerd, *Environ. Dev. Sustainability*, 2021, **23**, 6047–6065.
- 45 V. Vinayak, K. M. Manoylov, H. Gateau, V. Blanckaert, J. Hérault, G. H. Pencreac, J. Marchand, R. Gordon and B. Schoefs, *Mar. Drugs*, 2015, **13**, 2629–2665.
- 46 M. J. Khan, N. Bawra, A. Verma, V. Kumar, A. Pugazhendhi, K. B. Joshi and V. Vinayak, *Bioresour. Technol.*, 2021, **319**, 124129.
- 47 K. Herbach, F. Stintzing and R. Carle, *J. Food Sci.*, 2004, **69**, C491–C498.
- 48 R. Ramanarayanan, P. Nijisha, C. V. Niveditha and S. Sindhu, *Mater. Res. Bull.*, 2017, **90**, 156–161.
- 49 N. I. Beedri, S. A. A. R. Sayyed, S. R. Jadhkar and H. M. Pathan, *AIP Conf. Proc.*, 2017, **1832**, 040022.
- 50 Z. Hu, Y. Li, M. Sommerfeld, F. Chen and Q. Hu, *Eur. J. Phycol.*, 2008, **43**, 365–376.
- 51 D. V. Pogozhev, M. J. Bezdek, P. A. Schauer and C. P. Berlinguette, *Inorg. Chem.*, 2013, **52**, 3001–3006.
- 52 V. Hong and R. E. Wrolstad, *J. Agric. Food Chem.*, 1990, **38**, 708–715.
- 53 J. B. Harborne, *Biochem. J.*, 1958, **70**, 22–28.
- 54 D. L. Macuvele, G. Z. Sithole, K. Cesca, S. L. Macuvele and J. V. Matsinhe, *Environ. Sci. Pollut. Res. Int.*, 2016, **23**, 11639–11644.
- 55 A. Ahirwar, G. Meignen, M. J. Khan, V. Sirotiya, M. Scarsini, S. Roux, J. Marchand, B. Schoefs and V. Vinayak, *Bioresour. Technol.*, 2021, **340**, 125707.
- 56 H. Sun, Q. Kong, Z. Geng, L. Duan, M. Yang and B. Guan, *Bioresource technology*, 2015, **186**, 67–73.
- 57 Y. Nakamura, M. Hidaka, H. Masaki, H. Seto and T. Uozumi, *Agric. Biol. Chem.*, 1990, **54**, 3345–3346.
- 58 S. S. L. Priya, P. R. Devi, P. Eganathan and J. Kingsley, *Afr. J. Pharm. Pharmacol.*, 2013, **7**, 1719–1728.
- 59 K. Chekanov, D. Litvinov, T. Fedorenko, O. Chivkunova and E. Lobakova, *Biology*, 2021, **10**, 643.
- 60 P. Suganyadevi, M. Saravanakumar, K. Aravinthan, A. Arunkumar, R. K. Krishna and S. Karthikeyani, *J. Pharm. Res.*, 2010, **3**, 2693–2696.
- 61 D. Monchaud, J. Lacour, C. Coudret and S. Fraysse, *J. Organomet. Chem.*, 2001, **624**, 388–391.
- 62 A. Younas, S. Kiran, S. Abrar, S. Javed and T. Gulzar, *Pol. J. Environ. Stud.*, 2022, **31**, 5945–5954.
- 63 H. A. Pantami, M. S. Ahamad Bustamam, S. Y. Lee, I. S. Ismail, S. M. Mohd Faudzi, M. Nakakuni and K. Shaari, *Mar. Drugs*, 2020, **18**, 367.
- 64 M. S. A. Bustamam, H. A. Pantami, A. Azizan, K. Shaari, C. C. Min, F. Abas, N. Nagao, M. Maulidiani, S. Banerjee and F. Sulaiman, *Mar. Drugs*, 2021, **19**, 139.
- 65 R. Ranga, A. R. Sarada, V. Baskaran and G. A. Ravishankar, *J. Microbiol. Biotechnol.*, 2009, **19**, 1333–1341.
- 66 C. Jeffryes, J. Campbell, H. Li, J. Jiao and G. Rorrer, *Energy Environ. Sci.*, 2011, **4**, 3930–3941.
- 67 D. Zhang, Y. Wang, J. Cai, J. Pan, X. Jiang and Y. Jiang, *Chin. Sci. Bull.*, 2012, **57**, 3836–3849.
- 68 C. Jeffryes, T. Gutu, J. Jiao and G. L. Rorrer, *J. Mater. Res.*, 2008, **23**, 3255–3262.
- 69 S. Ito, T. N. Murakami, P. Comte, P. Liska, C. Grätzel, M. K. Nazeeruddin and M. Grätzel, *Thin Solid Films*, 2008, **516**, 4613–4619.
- 70 K.-H. Park, H.-B. Gu, E. M. Jin and M. Dhayal, *Electrochim. Acta*, 2010, **55**, 5499–5505.
- 71 S. Gupta, M. Kashyap, V. Kumar, P. Jain, V. Vinayak and K. B. Joshi, *J. Mol. Liq.*, 2018, **249**, 600–608.
- 72 Y. Qin and Q. Peng, *Int. J. Photoenergy*, 2012, **2012**, 1–21.

